Journal of Microscopy, Vol. 233, Pt 1 2009, pp. 149–159
Received 18 January 2008; accepted 18 July 2008

Confocal mosaicing microscopy in skin excisions: a demonstration of rapid surgical pathology

D.S. GAREAU*,‡, Y.G. PATEL*,‡, Y. LI†, I. ARANDA†, A.C. HALPERN*, K.S. NEHAL* & M. RAJADHYAKSHA*
**Dermatology Service, Room 230, Memorial Sloan-Kettering Cancer Center, 160 East 53rd Street, New York, NY 10022, U.S.A.*
†Memorial Sloan-Kettering Cancer Center, Research Engineering Laboratory, 1275 York Avenue, New York, NY 10021, U.S.A.

Key words. Acetowhitening, basal cell carcinomas, confocal microscopy, Mohs surgery, mosaicing.

Summary

Precise micro-surgical removal of tumour with minimal damage to the surrounding normal tissue requires a series of excisions, each guided by an examination of frozen histology of the previous. An example is Mohs surgery for the removal of basal cell carcinomas (BCCs) in skin. The preparation of frozen histology is labour-intensive and slow. Confocal microscopy may enable rapid detection of tumours directly in surgical excisions with minimal need for frozen histology. Mosaicing of images enables observation of nuclear and cellular morphology in large areas of surgically excised tissue. In skin, the use of 10–1% acetic acid as a reflectance contrast agent brightens nuclei in 0.5–5 min and enhances nuclear-to-dermis contrast and detectability of BCCs. A tissue fixture was engineered for precisely mounting surgical excisions to enable mosaicing of 36 × 36 images to create a field of view of 12 × 12 mm. This large field of view displays the excision at 2× magnification, similar to that routinely used by Mohs surgeons when examining frozen histology. Comparison of mosaics to histology demonstrates detectability of BCCs. Confocal mosaicing presently requires 9 min, instead of 20–45 min per excision for preparing frozen histology, and thus may provide a means for rapid pathology-at-the-bedside to expedite and guide surgery.

Correspondence to: Daniel S. Gareau. Tel: (212) 610 0832; fax: (212) 308 0739; e-mail: gareaud@mskcc.org

‡Both authors contributed equal effort to this research

Disclosure: *Milind Rajadhyaksha is a former employee of Lucid Inc., the company that makes and sells the VivaScope confocal microscope. He owns stock options in Lucid. The VivaScope is the commercial version of an original laboratory prototype of a confocal scanning laser microscope that was developed by Rajadhyaksha when he was in the Department of Dermatology at Massachusetts General Hospital, Harvard Medical School.*

Introduction

Precise micro-surgical removal of tumour with minimal damage to the surrounding normal tissue requires a series of excisions. Each excision is guided by an examination of the frozen histology of the previous. Examples include Mohs surgery for the removal of basal cell carcinomas (BCCs) in skin, excisions of mucosal lesions, thyroid nodules, parathyroid glands and bone during oral and head-and-neck surgery, needle-core biopsies and lumpectomies of breast, and biopsies of liver, bladder and many other tissues.

Mohs surgery requires one to two excisions, in general, and several in the case of large and complex BCC tumours. The preparation of frozen sections is labour-intensive and slow, requiring 20–45 min per excision during which the patient must wait under local anaesthesia and with an open wound (Rajadhyaksha *et al.*, 2001). Mohs surgery thus lasts 1–2 h, in general, and up to several hours for large and complex tumours. The need for frozen histology may be minimized and Mohs surgery expedited with the use of confocal microscopy to non-invasively examine thin optical sections. The optical section thickness of 1–3 μm and lateral resolution of 0.5–1.0 μm with confocal microscopy is comparable to that of standard histology. Nuclear and cellular morphology is non-invasively imaged in skin, either *in vivo* or in freshly excised or biopsied tissue *ex vivo*, without any of the processing that is necessary for histology. Confocal microscopy at high resolution is limited to small fields of view of 0.2–1 mm, whereas Mohs surgical excisions are relatively larger and usually 10–20 mm in size. However, mosaicing of a two-dimensional matrix of confocal images enables display of large fields of view and may enable rapid detection of BCCs in large excisions.

In our initial work, we demonstrated the feasibility of confocal mosaicing for rapid detection of BCCs in skin excisions of up to 10 mm in size (Rajadhyaksha *et al.*, 2001; Chung

et al., 2004). Acetic acid was used as a contrast agent to brighten nuclei in reflectance mode. The brightening of nuclei is the underlying mechanism for the clinically well-known acetowhitening phenomenon, which causes dysplastic mucosal epithelium to appear relatively 'whiter' or brighter than normal epithelium (Burghardt, 1959; Smithpeter *et al.*, 1998; Drezek *et al.*, 2000). The contrast of BCCs relative to the surrounding dermis was enhanced with acetowhitening by immersing skin excisions in acetic acid of concentration 5% for 30 s. Acetowhitening was determined to cause compaction of chromatin, which increases light back-scatter and makes the nuclei appear bright and easily detectable (Rajadhyaksha *et al.*, 2001, 2004; Chung *et al.*, 2004). When illuminated with linearly polarized light, the back-scattered light from the compacted chromatin was found to be somewhat more randomly polarized than that from the surrounding cytoplasm and dermis. Cross-polarization suppressed light back-scatter from the cytoplasm and dermis relatively more than that from the acetowhitened nuclei. Thus, the nuclear-to-cytoplasm contrast and BCC-to-dermis contrast appeared slightly more enhanced in cross-polarized images than that in brightfield images (Patel *et al.*, 2007). Our early mosaics displayed a large field of view of 10 mm, which is equivalent to magnification of 2×. However, the mosaics were limited by poor resolution, poor contrast and inconsistent image quality. This limited the ability to consistently visualize the edges of the excision, the epidermal margin and to detect BCCs including, especially, small tumours (Chung *et al.*, 2004).

In this paper, we report advances in instrumentation, particularly a tissue fixture to mount fresh surgical excisions, and the development of an imaging algorithm to overcome the early limitations and produce consistently high-quality confocal mosaics. Visual correlation of the confocal mosaics to the corresponding Mohs frozen histology is shown to be excellent. The cross-polarized mode of contrast provides small improvements in contrast and overall appearance of mosaics, as compared with those in the brightfield mode. Clinical implementation during Mohs surgery will require rapid acetowhitening followed by rapid mosaicing. The results of a pre-clinical study are reported that shows brightening and detectability of nuclei within 0.5–5 min when the excisions are immersed in acetic acid of concentrations 10–1%.

Materials and methods

Collection and preparation of Mohs surgical excisions

Skin excisions from Mohs surgery were obtained from the Mohs Surgery Unit in the Dermatology Service at Memorial Sloan-Kettering Cancer Center (MSKCC) following approval from the Institutional Review Board (IRB). During surgery, each excision is processed by the Mohs technician and three to four frozen sections are prepared, each section being about 5–6 μm thin. After the Mohs surgeon has examined the frozen sections, the remainder of the excision is discarded. These discarded excisions were collected. Our research, therefore, did not compromise standard Mohs procedures and did not affect routine patient care. Often, triangular-shaped slivers of normal skin are excised during wound closure to optimize cosmetic-reconstructive outcomes. These slivers are called 'dog-ears' because of their shape and are discarded after surgery. Fresh excisions of normal dog ear skin were also collected soon after they were discarded.

The collected Mohs excisions were frozen in the embedding medium that was used to prepare histology sections. Each excision was thawed from the embedding medium, rinsed with lukewarm water for few seconds, placed in a vial of isotonic potassium phosphate monobasic–sodium hydroxide buffer solution and then refrigerated. The excisions were living, as confirmed by viability staining with fluorescein diacetate and subsequent imaging of the fluorescein-labelled cellular cytoplasm (M. Rajadhyaksha, unpublished data).

Acetowhitening

Each Mohs excision was imaged with a confocal microscope prior to acetowhitening (i.e., control) and after acetowhitening. For the control, the thawed Mohs excision in the PBS solution was imaged. The excision was then acetowhitened by immersing in acetic acid prior to further imaging. To determine the conditions for optimum acetowhitening, a range of concentrations of acetic acid and a range of immersion times were tested. The tested concentrations were 10, 5, 3, 2 and 1% for immersion times of 5, 3, 2, 1 and 0.5 min, respectively. For each combination of acetic acid concentration and immersion time, five excisions were imaged for repeatability, resulting in a total of 125 excisions. The confocal images were visually evaluated and the minimum time was determined for brightening of nuclei and detectability of BCCs. The evaluation was limited to only the exposed surface of the excisions since the Mohs surgeon mainly needs to determine the lateral extent of tumour on the excised surface.

Mohs excisions are typically of size 10–20 mm and thickness 1–2 mm such that the tissue volume is no more than about 1 mL (assuming 60–70% content of the tissue being water). The excisions were immersed in 15 mL of acetic acid. Hence, the ratio of volume of contrast agent (acetic acid) to volume of tissue was 15:1. The relatively low concentrations of acetic acid and short immersion times do not affect the compliance of the tissue nor affect the preparation of frozen sections for histology, as verified and reported in the initial studies (Rajadhyaksha *et al.*, 2001; Chung *et al.*, 2004). Low concentration of acetic acid, when used in the clinic for acetowhitening, is usually rinsed out of the tissue prior to preparation of frozen histology. Note, however, that at much higher concentrations such as 50%, acetic acid acts

as a fixative. High-concentration acetic acid is used for fixing tissues (Fraschini *et al.*, 1981).

Because of the large volume ratio of 15:1, the excision is fully immersed with the exposed surfaces fully in contact with the acetic acid. The topical exposure of the acetic acid to the surface of the relatively large excision is uniform and complete. This ensures rapid diffusion of the acetic acid into the superficial layers of the excision that are the layers to be imaged for detecting BCCs to guide Mohs surgery. The diffusion coefficient, D, of acetic acid into water is 1.29×10^{-5} cm^2s^{-1} (*The Biomedical Engineering Handbook*, 1995; *CRC Handbook of Chemistry and Physics*, 1998–1999). Across a semi-infinite slab of thickness L, the diffusion time is $L^2/2D$. A layer of cells on the surface of the excision is about 10 μm thick. Hence, the estimated diffusion time into the first layer of cells is approximately 40 ms. Considering the very rapid diffusion into the cellular layer to be imaged, the immersion time represents the time required for subsequent compaction of chromatin and brightening of nuclei and detectability of BCCs.

Confocal microscope instrumentation

The imaging was performed with a modified laboratory version of a commercial reflectance confocal microscope (Vivascope 2000, Lucid Inc., Rochester, New York). The microscope is in an inverted configuration and designed specifically for imaging fresh tissue excisions *ex vivo*. The design and instrumentation details were reported earlier (Rajadhyaksha *et al.*, 2001; Chung *et al.*, 2004; Patel *et al.*, 2007). Briefly, the illumination is at a near-infrared wavelength of 830 nm and with low power of 1–5 mW on the tissue. The objective lens is a 30×, 0.9 numerical aperture (NA) water immersion (StableView, Lucid Inc., Rochester, New York) that was custom designed to image through a standard 1-mm-thick glass slide. This lens provides a field of view of 430 μm. The nominal diffraction-limited lateral resolution is 0.7 μm and optical section thickness is 2 μm. The detection pinhole diameter is 150 μm, which corresponds to 5 times the nominal lateral resolution. The illumination laser beam is linearly polarized (p state) and detection is through a cross polarizer (s state). By rotation of a quarter-wave plate behind the objective lens, the imaging mode of contrast may be switched between brightfield and cross-polarized. Images are captured with an image acquisition board (Imaq 1408, National Instruments Inc., Austin, Texas) at a rate of 15 $frames^{-1}$.

As in previous studies, water as an immersion medium was often substituted with water-based commercial hair gels such as Vidal Sassoon® or Suave® (Rajadhyaksha *et al.*, 1999, 2001; Patel *et al.*, 2007). Gels are especially convenient to use in microscopes that have inverted objective lens configurations. These hair gels are of refractive index 1.34, which is reasonably close to that of water (1.33). Another commonly available alternative is Aquasonic 100 gel, which is clinically used for ultrasound imaging. This gel has a slightly higher refractive index of 1.36 but may be diluted in 1:2 ratio with water to reduce the refractive index to 1.34. The use of such gels does not degrade the image quality of the superficial tissue layers. The immersion gel is placed between the objective lens and the glass slide, whereas the skin excision is kept hydrated with isotonic phosphate-buffered solution. Once the excision was placed in the tissue fixture, properly positioned and oriented, and the illumination power adjusted, confocal images and mosaics were captured.

The surface of the excision is imaged and mosaiced. The frozen excision is thawed, rinsed, acetowhitened and mounted in a tissue fixture prior to imaging. Consequently, small distortions of the imaged surface may be expected owing to the compliance of the tissue. Thus, the images and mosaics are expected to show a close but not exact correlation to the frozen histology sections that were prepared during surgery by the Mohs technician.

Tissue fixture

Fresh excisions from surgery are living, hydrated, compliant and of complex and irregular shapes and geometries. Such surgical excisions are therefore not easy to mount for confocal microscopy. To enable confocal mosaicing for visualization of large fields of view, we engineered a special tissue fixture to mount Mohs surgical excisions (Fig. 1). The fixture allows repeatable and accurate control of the flattening, tip, tilt, sag and stability of the surface to be imaged. The functionality of the tissue fixture mimics the operation of cryostats that are routinely used for preparing frozen histology sections for Mohs surgery.

The tissue fixture encompasses the inverted 30×, 0.9-NA water-immersion objective lens of the VivaScope confocal

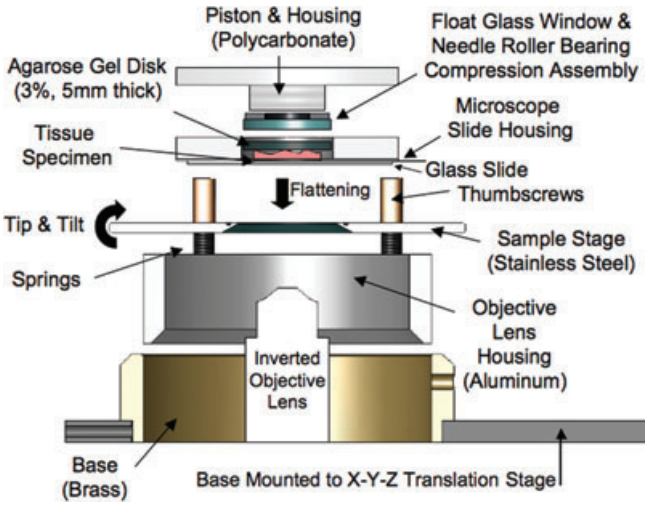

Fig. 1. Tissue fixture for mounting surgical skin excisions.

microscope (Lucid Inc., Rochester, NY, U.S.A.). The objective lens is custom-designed to image through a 1-mm-thick glass slide. Capturing a two-dimensional matrix of images to create mosaics of the large excisions requires the fixture to gently flatten and accurately position and orient the surface of the excision that is to be imaged. This requires gentle and uniform pressure on the excision, with user-adjustable tip, tilt and objective lens-to-excision distance. This is analogous to the user-controlled positioning and orientation of the excision in the cryostat by Mohs technicians when preparing frozen histology sections. Once the excision is placed on the glass slide, a piston is used to gently apply pressure on the top to flatten the lower surface. The 1-mm-thick glass slide is stiff enough to prevent the lower surface (i.e. tissue surface to be imaged) from sagging under the pressure of the piston. (Standard 170-μm-thin cover slips that are normally used with objective lenses do not work as well. The thin cover slips either sag or break such that capturing a two-dimensional matrix of images over a large area is not possible.) The tip, tilt and orientation of the glass slide relative to the objective lens are adjusted with spring-loaded thumbscrews. This is similar to the kinematic mount that is commonly used in optics.

To ensure uniform pressure and flattening of the lower surface, a mechanically compliant material is necessary between the piston and the irregular shape of the excision. We use cold-form agarose gel discs. Agarose solution of concentration 3% in warm water is placed in (custom-made) circular Delrin plastic molds and cooled to room temperature. Under the piston-induced pressure, the gel conforms to the shape of the excision, which subsequently becomes embedded within the disc. This is analogous to the embedding of skin excisions in the cryostat for preparing Mohs frozen histology. Agarose gel concentrations of 1–5% with disc thickness of 1–5 mm were empirically tested. With concentrations of 1 and 2%, the discs were too fragile and crumbled under the pressure of the piston. With concentrations of 4 and 5%, the discs were too stiff and did not conform to the excision. With concentration of 3%, the agarose gel discs conformed to the excision without breaking. Discs of thickness 1 mm crumbled, whereas those of thickness 2–5 mm did not.

When the piston is rotated to apply pressure on the embedded excision within the gel disc, the edges of the tissue tend to twist and distort. This rotation-induced twisting of the tissue is prevented by placing a thin polycarbonate disc and needle-roller bearings (Part number 5909K31, McMaster-Carr, New Jersey) between the piston and the gel disc. The tissue fixture encompasses the objective lens and is mounted onto the three-dimensional *xyz* translation stage of the confocal microscope with user-controlled height adjustment. The fixture is robust and allows accurate and repeatable imaging and mosaicing. (The authors will freely share engineering drawings and further details of the design, manufacturing and operation of the tissue fixture with researchers who may be interested.)

Acquisition of mosaics

Skin excisions from Mohs surgery are typically 10–20 mm, whereas the field of view with the current 30× objective lens is 0.43 mm. (More recently available lenses with lower magnification such as Nikon 20×/0.75 NA (Nikon Inc., Melville, NY, U.S.A.), Olympus 20×/0.95 NA (Olympus Inc., Center Valley, PA, U.S.A.) and Lucid 10×/0.8 NA (Lucid Inc.) provide increased field of view of 0.75–1.00 mm and may prove useful in future work for large area mosaicing.) To observe large areas of an excision, a two-dimensional matrix of images is captured and stitched in software to create a mosaic that displays a large field of view. The mosaicing was limited to only the exposed surface of the excisions since the Mohs surgeon requires mainly a lateral map of the extent of tumour on the excised surface. The matrix of images is acquired with a continuous step-and-capture routine while translating the tissue fixture with stepper motors–driven linear XY stages (Hayden Inc., Stamford, Connecticut). Depending on the size of an excision, 10–20% overlap was deliberately included in the translation step distance so as to not miss any areas of tissue near the edges of the field of view. The amount of cropping may be adjusted according to the size of the excision, since there is a trade-off between the amount of overlap and mosaicing speed. Acquisition of the matrix of images and preparation of mosaics was accomplished with two PCs that were connected through MSKCC's internal network. Images were captured using Lucid's Vivascope software by the PC that controlled the confocal microscope. The images were then immediately transferred to the second PC for archiving and processing. This set-up enabled the Vivascope's PC to continue rapidly capturing matrices of images from each excision that was received from the Mohs surgery unit, whereas, in parallel, the second PC created mosaics of the previous excisions. Approximately 100 mosaics were created during the development and testing of the tissue fixture and mosaicing algorithm.

Image-stitching algorithm to create mosaics

Mosaics were created with MATLAB software (version 7.0.1, MathWorks, Natick, Massachusetts). The algorithm to create mosaics implements the following steps: correction for the effects of field curvature, cropping of the overlap between images, merging of images into a single composite image and correction for the effects of illumination vignetting. Field curvature results in the illumination and imaging not of a plane but of a curved surface such that a faint circular ring was present at the edges in each of the images. The ring occurs owing to reflection from the glass slide that is contact with the underlying tissue. The field curvature was corrected by subtracting a reference image of the ring from all original images. The reference image was of the glass slide without any underlying tissue. Following this correction, images were cropped to correct for the overlap at the edges. The

amount of cropping was pre-defined by the stepping distance of the XY translation stages during the image acquisition, and further precisely adjusted by measurements of overlap using image analysis software (IPLab Spectrum, version 3.6.5, BD Biosciences, Inc., Rockville, Maryland). Based on our experience, the overlap between images remained repeatedly consistent across large mosaics with minimal errors. After cropping, the images were merged or concatenated into a single composite mosaic. In the following step, shading bands at the edges between pairs of neighbouring images were corrected for with inverted brightness polynomial fits, to correct for illumination vignetting effects. The brightness or pixel greyscale values are defined as $I(x, y)$. Across the dark band at each edge (between a given pair of neighbouring images) that is, say, in the y direction, the mean brightness (i.e. mean pixel greyscale values) profile as a function of x pixel location is determined. The mean brightness profile is defined as $I_{\text{mean}}(x)$. The median value across the profile is I_{median}. The inverted brightness polynomial to correct for the shading bands is given by $I_{\text{correction}}(x) = I_{\text{median}} - I_{\text{mean}}(x)$. The correction that is applied to the pixel greyscale values is $I_{\text{corrected}}(x, y) = I(x, y) + I_{\text{correction}}(x)$. When I_{mean} is larger than I_{median}, which mostly occurs outside the shading bands, there is no correction necessary and $I_{\text{correction}}(x) = 0$. Following the inverted brightness polynomial fit, any residual dark stripes, which were mostly in the form of thin dark lines at the edges, were reduced with a destripe filter. The destripe filter was developed by Marc Lehman as an open-source software called GNU Image Manipulation Program (GIMP), version 2.2 (GIMP, Free Software Foundation Inc., Boston, MA, U.S.A.). Executable and source code may be downloaded at www.GIMP.org. The destripe filtering routine follows an algorithm that is similar to that of the inverted polynomial fit. There are two differences, however. One is that the destripe filter operates on the edges of the entire mosaic, instead of individual pairs of images. The mean brightness (i.e. mean pixel greyscale values) profile as a function of x pixel location across the entire mosaic is determined as $I_{\text{mean,mosaic}}(x)$. The second difference is that a low-pass filter is applied to the mean pixel brightness profile to determine an average background brightness across the mosaic, $I_{\text{average,mosaic}}$. The correction that is then applied is $I_{\text{average,mosaic}} - I_{\text{mean,mosaic}}(x)$ across the entire mosaic. The processed mosaic is saved in TIFF format. (The authors will freely share the algorithm and MATLAB software, including implementation details, with researchers who may be interested.)

Display of mosaics

When examining frozen histology sections, with a 2×, 0.08-NA objective lens and white-light illumination (wavelength λ of about 0.5 μm), the Mohs surgeon observes a field of view of 10 mm with a resolution of approximately 4 μm. The observed field of view consists of 2500 × 2500 pixels, assuming one pixel per optical lateral resolution point. Thus, the confocal mosaics must be displayed with at least 2500 × 2500 pixels to ensure that the display resolution does not degrade the optical lateral resolution. We observe mosaics on a 21-inch cathode ray tube (CRT) monitor (ViewSonic Corporation, Professional Series P220*f*, Walnut, California) using visualization software (PhotoImpact, MicroTek, or IPLab Spectrum, version 3.6.5, BD Biosciences, Inc.). (Note that the mosaics and images may appear with severely degraded quality on certain liquid crystal display monitors owing to sub-optimal brightness, contrast and gamma settings.) The visualization software allows digital zooming to display sub-mosaics with increased magnification of 4× or 10×, which mimics the Mohs surgeon's use of 4× or 10× objective lenses to examine histology with higher magnifications.

Each image consists of 640 × 480 pixels, is 8-bit greyscale and requires about 1/4 MB of memory. Thus, a mosaic of 36 × 36 images at full resolution consists of 23040 × 17280 pixels and requires about 325 MB of memory. The processed mosaic is scaled down using bilinear interpolation to make the final display equivalent to a histology-like 2× view. The final displayed mosaic consists of 2500 × 2500 pixels and requires less than 4 MB.

Comparison of brightfield versus cross-polarized mosaics

The illumination laser beam in the Vivascope confocal microscope is linearly polarized (*p* state) and detection is through a cross-polarizer (*s* state). By rotation of a quarter-wave plate behind the objective lens, the imaging mode of contrast may be switched between brightfield and cross-polarized. Mosaics were acquired in both brightfield and cross-polarized modes and visually assessed for overall appearance and further compared for enhancement of nuclear-to-cytoplasm and BCC-to-dermis contrast.

Comparison of confocal mosaics to frozen histology

Comparison of confocal mosaics to the frozen histology was performed by our collaborating Mohs surgeon (co-author K.N.). Mosaics were assessed for overall image quality, appearance of tissue edges, presence of the epidermal margin, presence of normal dermal features and detectability (either presence or absence) of BCC tumour nests. As explained earlier, three to four frozen sections of each excision are routinely prepared during Mohs surgery, with standard hematoxylin and eosin (H&E) staining. These frozen histology sections were available for comparison to the confocal mosaics. The confocal images, mosaics and sub-mosaics were visually compared with the frozen histology at standard microscope magnifications of 2×–40×. In addition, differences in brightfield versus cross-polarized confocal mosaics were evaluated.

The exposed surface of the discarded excision was imaged. This is the exposed surface of the Mohs excision that remains (and is discarded) after the Mohs technician has performed cryostat sectioning to prepare frozen histology for the Mohs surgeon. The exposed surface represents the tissue immediately adjacent and deeper to the final section. When the frozen excision is thawed, rinsed, acetowhitened and mounted in the tissue fixture, distortions can occur owing to the mechanical compliance of tissue. Thus, a close but not identical correspondence was expected between the confocal mosaics of the exposed surface and the final section of frozen histology.

Results

Tissue fixturing and mosaicing algorithm enables rapid examination of surgical excisions

Of the approximately 100 mosaics that were created during this development work, 30 demonstrate repeatability of the tissue fixturing and mosaicing algorithm and significant improvement over our early methods. The algorithm results in mosaics that appear reasonably seamless and contiguous with high resolution and uniform illumination over large excisions, and are useful for clinical visualization and correlation to standard histology. Figures 2–4 of mosaics in this paper

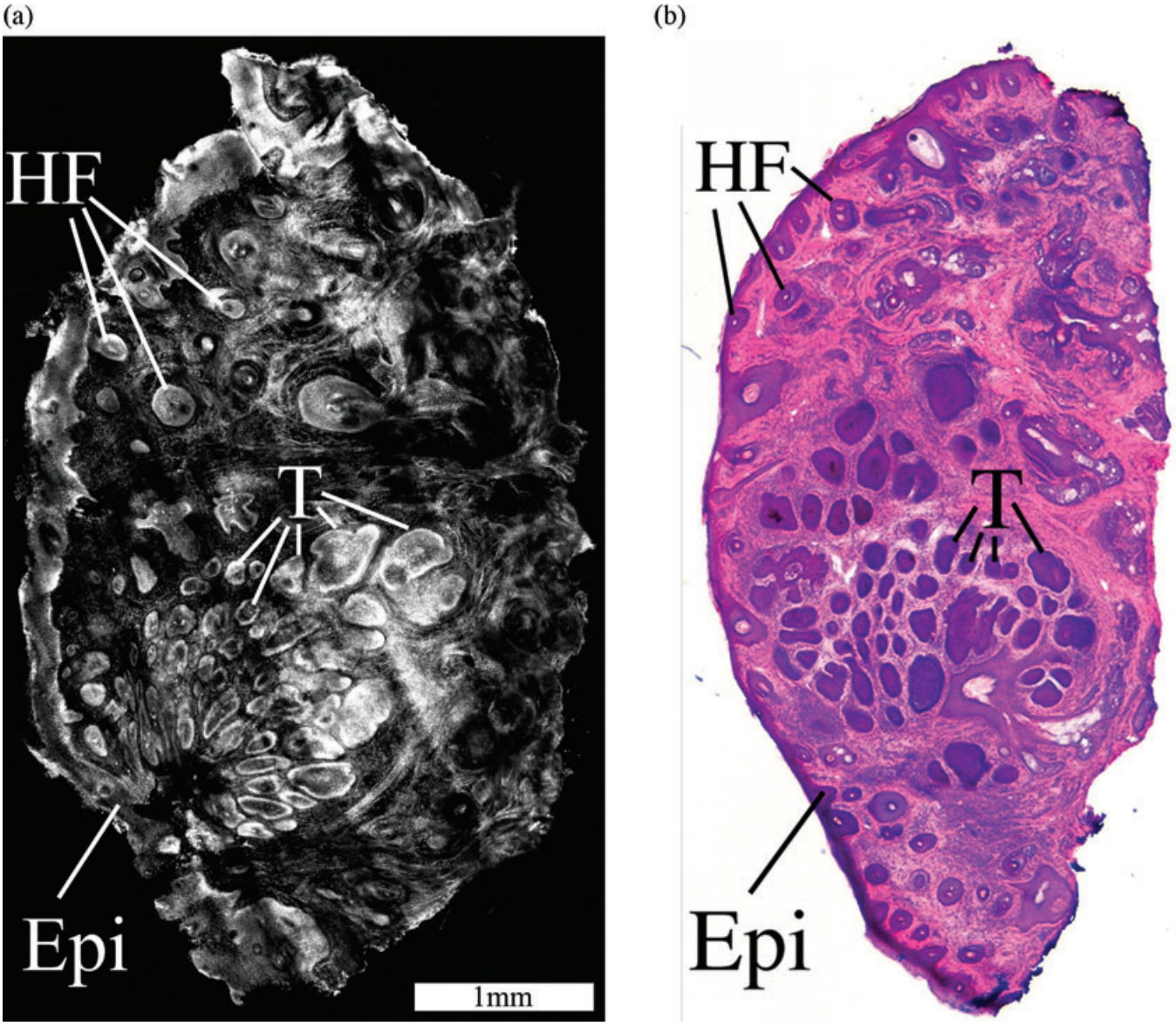

Fig. 2. Brightfield confocal mosaic (A) shows nodular BCC tumour at 2× magnification that compares well to the corresponding frozen histology (B). Nests of tumour (T) within the dermis, the epidermal margin (Epi) and hair follicles (H) are seen. Acetowhitening with 2% acetic acid for 2 min.

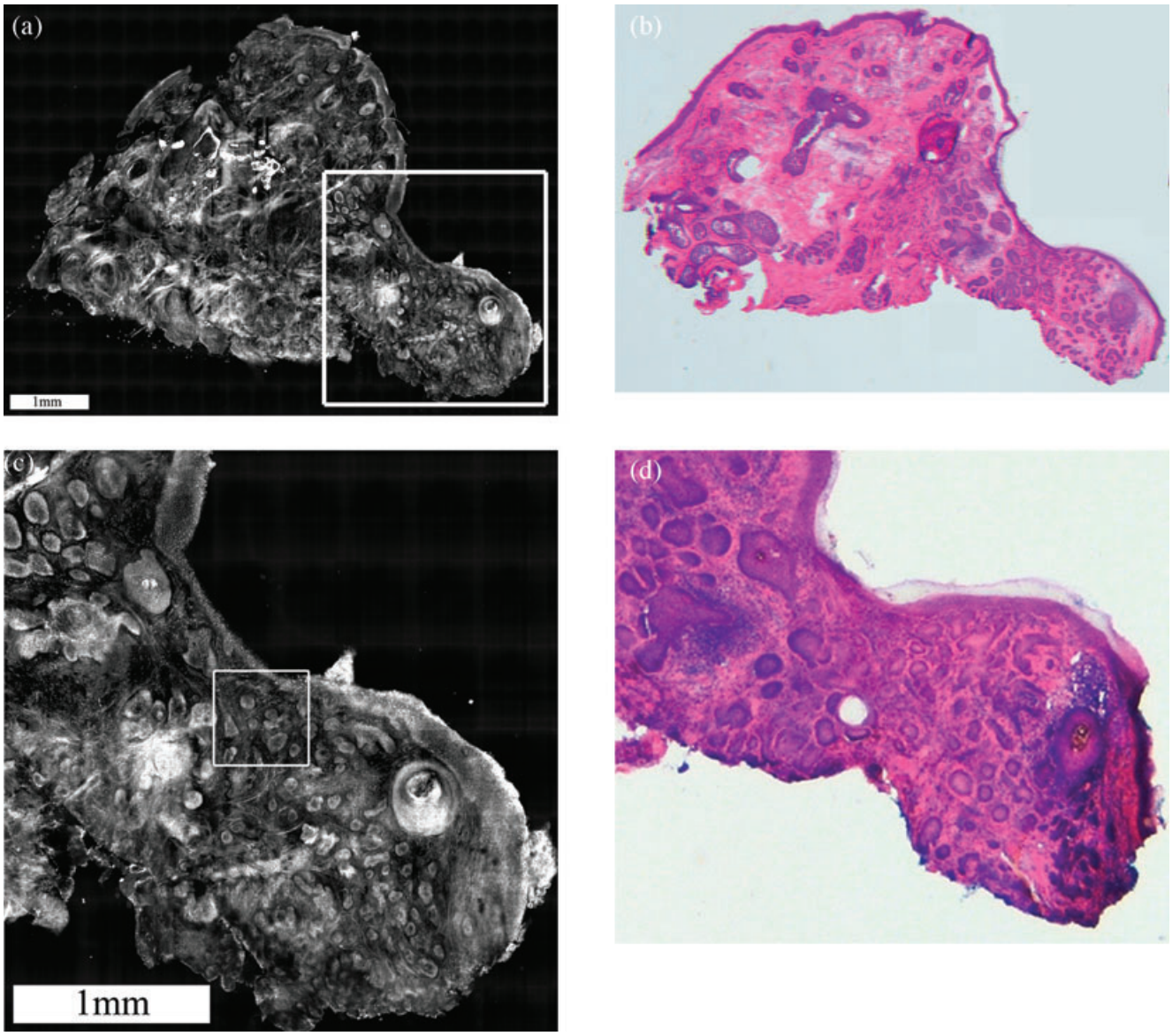

Fig. 3. Cross-polarized confocal mosaic (A) shows micro-nodular BCC tumour at 2× magnification that compares well with corresponding histology (B). The inset box shows a sub-mosaic at higher magnification of approximately 5× (C), and the corresponding frozen histology (D). Tumours (T) are seen within the dermis. Image (E) shows tumour nests with pleomorphic nuclei, palisading (P) at the peripheral inner edges and clefting (c) on the peripheral outer edges. Acetowhitening with 3% acetic acid for 1 min.

show the improvements in quality when compared with those shown from our earlier study (Chung *et al.*, 2004). The image quality of the mosaics was assessed by our Mohs surgeon (co-author K.N.) to be consistently high for examination of morphologic features that are clinically important for surgical pathology. In Mohs skin excisions, the features include the edges of the tissue, epidermal margins, normal dermis and nuclear detail and gross morphology of BCCs.

At present, up to 36 × 36 images are stitched together to display a field of view of up to 12 × 12 mm, which simulates magnification of 2×. Mohs surgeons routinely use an objective lens with 2× magnification to quickly examine large areas of frozen histology sections. Objective lenses with 4× and 10× magnifications are used, when necessary, for closer inspection of nuclear detail. Similarly, the entire confocal mosaic, as well as smaller portions called sub-mosaics, may be displayed to examine an excision at variable resolution and magnification. For acquisition of a mosaic, a continuous step-and-capture routine requires about 5 min for 36 × 36 images. Transferring and archiving images followed by processing to create a mosaic requires another 4 min on a PC with a Pentium III 1.2-GHz processor. Thus, total time to create a mosaic is 9 min at present. By comparison, preparation of frozen histology requires 20–45 min for an excision.

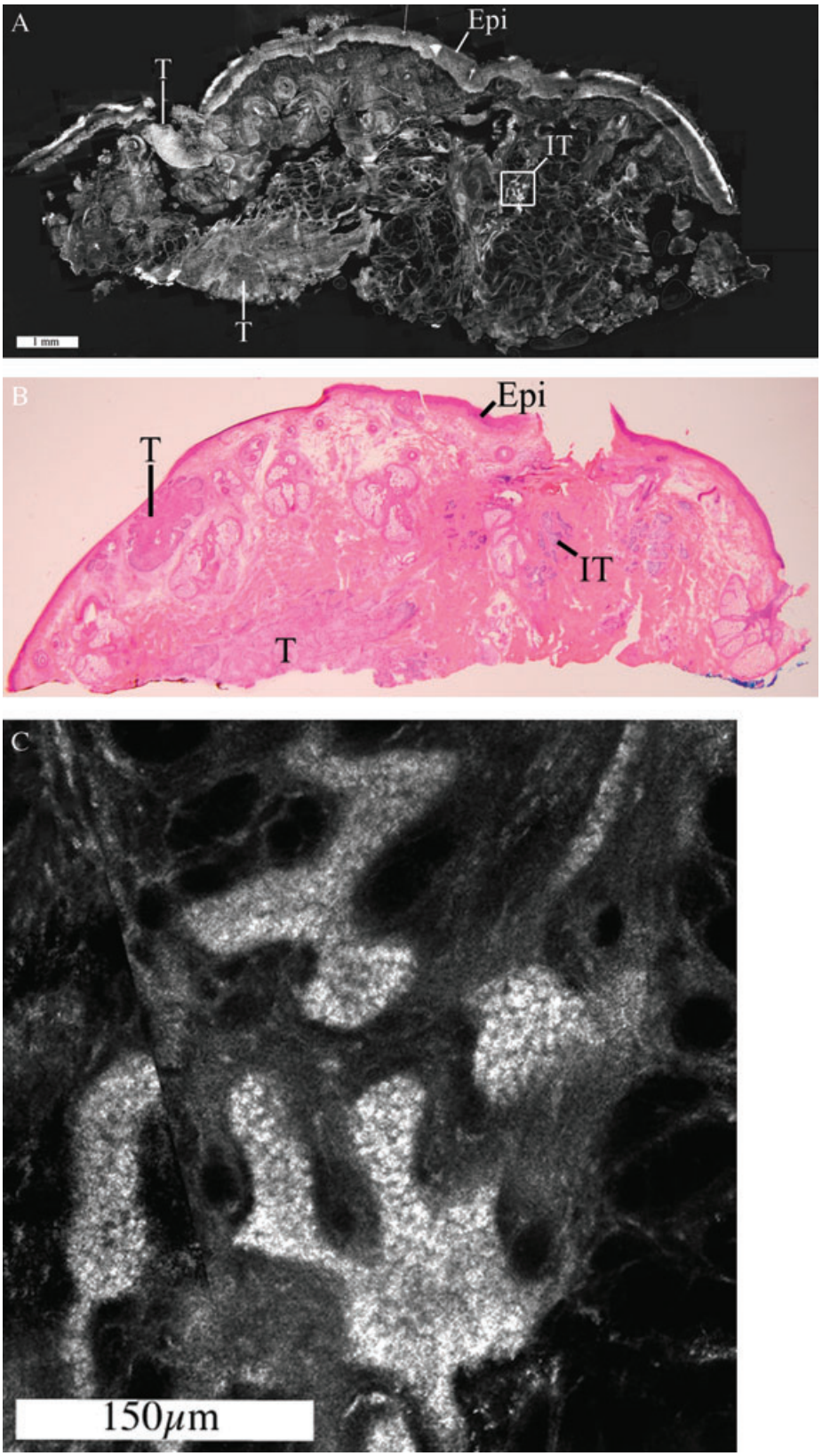

Fig. 4. Brightfield confocal mosaic (A) shows infiltrative BCC tumour and the corresponding histology (B). Nodular (T) and infiltrative (IT) types of tumours are seen. The inset box shows the infiltrative tumour at a magnification of 30× (C). Pleomorphic nuclear detail is seen in the tumour nests. Acetowhitening with 5% for 3 min.

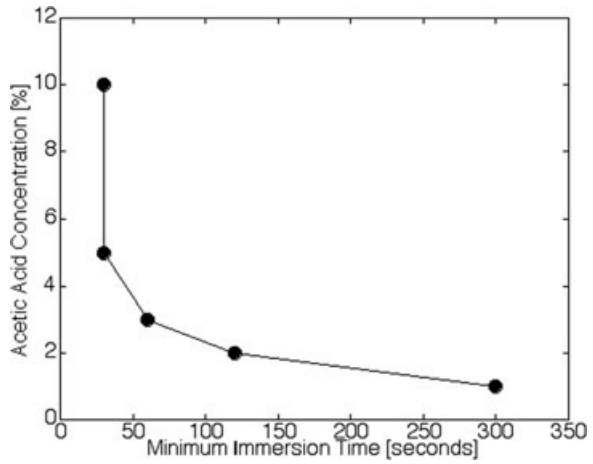

Fig. 5. Minimum immersion time versus concentration of acetic acid for brightening of nuclei (acetowhitening).

Acetowhitening rapidly brightens nuclei as a function of concentration and immersion time

Images of excised skin after immersion in acetic acid compared with those before (control) were reported in earlier work, demonstrating the brightening of nuclei due to acetowhitening (Rajadhyaksha *et al.*, 2001). Acetowhitening was also shown to not affect subsequent frozen histology with H&E staining.

Figure 5 shows that low concentrations of acetic acid with short immersion times are effective for brightening nuclei in Mohs excisions. Acetic acid concentrations of 10 and 5% require immersion times of only 30 s, whereas 3, 2 and 1% require 1, 2 and 5 min, respectively. Rapid brightening within 1 min is possible for concentrations of 3% and higher. The required concentration of acetic acid decreases as immersion time increases at a rate that suggests a first-order chemical reaction (Fig. 5). The brightening of the nuclei, as observed only on the exposed surface, was found to be independent of the size of the excisions. This is to be expected with the excisions being fully immersed in a large volume of acetic acid and due to the very rapid diffusion time of approximately 40 ms into the superficial layer of cells that was imaged.

Comparison of confocal mosaics to frozen histology demonstrates detectability of BCCs

Figures 2–4 show excellent comparison between confocal mosaics and the corresponding Mohs frozen histology for normal skin morphology and BCCs as validated by the Mohs surgeon. The epidermal margin of the excision along with the dermo-epidermal junction is clearly and repeatably identified on the mosaics. Normal structures in the dermis such as sebaceous glands, hair follicles and eccrine glands are easily and consistently visualized. The gross morphology of BCCs in terms of shape, size and location of tumour nests as seen in the mosaics corresponds well to that seen in frozen histology. In addition, the atypical morphology of nuclei in the BCC nests in terms of pleomorphism (varying shapes, sizes, orientations and irregular distributions), crowding (increased density) and palisading is clearly visualized in the mosaics and corresponds well to the histology. Inflammatory infiltrates are seen around BCC nests.

The nuclear detail appears bright and is clearly visible in the epidermal margin and in the BCCs within the dermis because of the acetowhitening. The acetowhitening strongly enhances BCC-to-dermis contrast and enables detectability of BCC tumour nests. Relatively large sub-types of BCCs, such as superficial, nodular and micro-nodular, are easily detected in the confocal mosaics and compare well to the histology. However, small sub-types of BCCs such as infiltrative and sclerosing are difficult to detect. These sub-types consist of very small nests or thin strands of nuclei that image with relatively weak contrast and tend to remain hidden within the surrounding bright collagen, especially in the deeper reticular dermis. Although such small nests and thin strands of nuclei are easily seen in individual images or small sub-mosaics, they are obscured and not detectable in the full-sized mosaics.

Cross-polarization suppresses the light back-scatter from the cytoplasm and dermis slightly more than that from the compacted chromatin. Small improvements in contrast were thus observed of the acetowhitened nuclei relative to the cytoplasm and of the BCC nests relative to the surrounding dermis. Furthermore, cross-polarization improves the overall contrast and appearance of the mosaics because of the suppression of background light reflections from the tissue fixture and particularly from the glass slide and agarose gel disc. Hence, the edges of the Mohs excision appear better delineated and the overall contrast between the BCC nests and the surrounding dermis appears better. Similar observations were reported earlier (Rajadhyaksha *et al.*, 2001; Patel *et al.*, 2007).

Discussion

The use of frozen histology to guide surgery requires a significant amount of labour, time and resources and accounts for 10–20% of the operating costs. New developments in confocal mosaicing microscopy show the potential for detection of tumours directly in surgical excisions without processing of the tissue. However, substantial advances are necessary to progress from the laboratory towards clinical utility.

Reflectance contrast with acetowhitening allows the detection of relatively large superficial-, nodular- and micro-nodular-type tumours in large area mosaics. A recent study reported high diagnostic accuracy of 100% for detection of BCCs (Gerger *et al.*, 2005). A later study (Horn *et al.*, 2007) on squamous cell carcinomas from 20 patients yielded sensitivity of 95% and specificity of 96%. However, these analyses were

based on pre-selected individual images (in which BCCs are easily seen at high magnification) rather than in mosaics.

The most important requirement for clinical utility is contrast agents that enable detection of tumours with widely variable morphology, especially those that occur in small or tiny sizes. Alternative modes of contrast such as fluorescence and autofluorescence, with more specific staining of nuclei or dermis, may prove to be more effective than reflectance. Two or more modes of contrast (i.e., multi-modal contrast) may be necessary: a 'positive' mode for detecting the presence of tumour and a 'negative' mode for detecting the absence of tumour (which means presence of normal tissue). This would be similar to the standard use of positive and negative stains in histology. Towards this goal, alternative modalities including multi-modal contrast are being investigated by several groups for imaging of BCCs.

Raman spectroscopy is a possible alternative modality. A linear discriminant analysis model was shown to accurately discriminate 19 nodular- and morphea-type BCC biopsies from nine perilesional skin samples (Nijssen *et al.*, 2007). Of the 19 samples, 9 contained tumour in less than half of the specimen, so the technique is sensitive to low tumour burden, but it is unclear how much must be present for detection. In the limit of one infiltrative or sclerosing tumour strand, spatial resolution may be necessary. In another study on excised specimens, spectral analysis algorithms were developed for 100% sensitivity and 100% specificity in 39 patients when collecting spectra from the stratum corneum (Lieber *et al.*, 2008). Deeper, including at the dermal-epidermal junction where the BCC originates, however, the classification accuracy was somewhat reduced. Nonetheless, using such spectroscopic methods shows promise to enhance tumour-specific contrast. Autofluorescence contamination, weak signals that require long detection times, sparse sampling and extensive data-processing requirements remain challenges to clinical use. Fluorescence contrast offers another alternative that may specifically stain tumour but not the dermis. Strong contrast with high specificity increases the detectability of the small micro-nodular and tiny infiltrative tumours. The nuclear stains methylene blue and toluidine blue have been used to provide strong fluorescent contrast to tumours (Al-Arashi *et al.*, 2007). In 30 cases of mixed BCCs and SCCs, confocal imaging showed good correlation with histopathology. In other studies by the same group, imaging using fluorescence polarization identified 79 out of 86 lesions correctly (Yaroslavski *et al.*, 2007). Similarly, combining aminolaevulinic acid (ALA)-induced protoporphyrin IX fluorescence and autofluorescence followed by Fisher linear discrimination and texture analysis showed good discriminability in 15 patients with BCCs (Ericson *et al.*, 2005). This technique is based on macroscopic mapping of lesions. The specificity of ALA-induced fluorescence alone was insufficient for discriminating BCC because of heterogeneous distributions in tumour areas although it provided useful information for the texture analysis. In another study (Stenquist *et al.*, 2006) from the same group, the correlation between the wide-field fluorescence imaging and histology was found to be good for 42% of the 12 patients and partial for the remaining 58%. Other work (Lin *et al.*, 2006) reported that the ratio of multi-photon fluorescence (which increases in tumours) to second-harmonic generation (which decreases in tumours) discriminated nine nodular BCC tumours from the surrounding dermal stroma. A study based on multi-photon fluorescence alone on 14 patients with mixed BCC and SCC showed that the traditional histopathological diagnostic criteria can clearly be observed (Paoli *et al.*, 2007). In another study, fluorescence lifetime imaging has demonstrated the ability to distinguish 25 BCC-affected areas from perilesional normal areas (Galletly *et al.*, 2008). Yet another modality is optical coherence tomography. Although with low lateral resolution, this technique shows promise as a pathological tool (Olmedo *et al.*, 2006). Similar to confocal microscopy, all these modalities appear promising in feasibility studies and either alone – or, most likely, in multi-modal combination – may prove useful for clinical applications.

The mosaicing must be made faster to enable further clinical studies, towards eventual application and acceptance by surgeons. Preliminary engineering analysis predicts that, with better-implemented hardware and software, mosaics of 20 × 20 mm may be created in about 2–3 min. The quality of the mosaics must be improved with more seamless stitching of images and better correction for illumination vignetting effects. Mosaics with perfectly (or near-perfectly) seamless stitching of images may be possible with lateral registration of images by matching features at the edges between images (Chow *et al.*, 2006; Sun *et al.*, 2006). Further pre-clinical studies are necessary to improve the Mohs surgeons' abilities to interpret mosaics, similar to their examination of frozen histology. As with any new imaging modality, 'image understanding' will be the most critical factor for translating confocal mosaicing from the laboratory into an accurate and repeatable instrument in the clinic.

Beyond our immediate work on skin cancers, confocal mosaicing microscopy may enable real-time surgical pathology in many other tissues with high-impact high-value outcomes to overcome the time delays, limited sampling, limited accuracies and high costs of today's histology procedures. Examples include needle-core biopsies and lumpectomies of breast tissue, excisions of thyroid and parathyroid during head-and-neck surgery, excisions of mucosal lesions and bone during oral mandibulectomies and excised tissue from many other surgical settings.

Summary and conclusions

Confocal reflectance mosaicing may enable rapid detection and examination of BCCs in skin excisions from Mohs surgery.

At present, mosaics are produced in 9 min, compared with 20–45 min required per excision for preparing frozen histology sections. Mosaics and sub-mosaics enable observation of large areas of excised tissue with variable resolution, magnification and field of view, in a manner that is similar to the Mohs surgeon's examination of frozen histology. Detectability of nuclear detail requires the mosaic resolution and the display pixelation to equal or exceed that of a 2×-magnified view of histology. With further advances in the instrumentation and multi-modal forms of contrast, confocal mosaicing microscopy may evolve into a technology for rapid pathology at the bedside to potentially expedite and guide surgery.

Acknowledgements

The authors thank Mohs histology technicians Marie Tudisco and Barbara Strippoli for supplying discarded excisions from Mohs surgeries, help with the frozen histology and their intellectual involvement with all aspects of this research. The authors are grateful to Dr. Jay Eastman and William Fox of Lucid Inc. for their technical support. This work was funded mainly by National Institutes of Health grant R01EB002715 from the Image-Guided Interventions program of the National Institute of Biomedical Imaging and Bioengineering (Program Officer Dr. John Haller). Additional funding was provided by a grant from the Byrne Fund (Department of Medicine at MSKCC).

References

The Biomedical Engineering Handbook. (1995) (J.D. Bronzino, Editor-in-Chief), pp. 1661–1664, CRC Press, New York.

CRC Handbook of Chemistry and Physics. (1998–1999) (D.R. Lide, Editor-in-Chief), 79th edition, pp. 6–181, CRC Press, New York.

Al-Arashi, M.Y., Salomatina, E. & Yaroslavsky, A.N. (2007) Multimodal confocal microscopy for diagnosing nonmelanoma skin cancers, Laser. *Surg. Med.* 39, 696–705.

Burghardt, E. (1959) Uber die atypische Umwandlungszone. Geburtsh U Frauenheilk 19, 676.

Chow, S.K., Hakozaki, H., Price, D.L., *et al.* (2006) Automated microscopy system for mosaic acquisition and processing. *J. Microsc.* 222, 76–84.

Chung, V.Q., Dwyer, P.J., Nehal, K.S., Rajadhyaksha, M., Menaker, G.M., Charles, C. & Jiang, S.B. (2004) Use of *ex vivo* confocal scanning laser microscopy during Mohs surgery for non-melanoma skin cancers, dermatol. *Surgery* 30, 1470–1478.

Drezek, R.A., Collier, T., Brookner, C.K., Malpica, A., Lotan, R., Richards-Kortum, R.R. & Follen, M. (2000) Laser scanning confocal microscopy of cervical tissue before and after application of acetic acid. *Am. J. Obstet. Gynecol.* 182, 1135–1139.

Ericson, M.B., Uhre, J., Strandeberg, C., Stenquist, B., Larko, O., Wennberg, A.M. & Rossen, A. (2005) Bispectral fluorescence imaging combined texture analysis and linear discrimination correlation with histopathologic extent of basal cell carcinoma. *J. Biomed. Opt.* 10(034009), 1–8.

Fraschini, A., Pelliciari, C., Biggiogera, M. & Romanini, M.G.M. (1981) The effect of different fixatives on chromatin: cytochemical and ultrastructural approaches. *Histochem. J.* 13, 763–779.

Galletly, N.P., McGinty, J., Dunsby, C., *et al.* (2008) Fluorescence lifetime imaging distinguishes basal cell carcinoma from surrounding uninvolved skin. *Br. J. Dermatol.* **159**, 152–161.

Gerger, A.G., Horn, M.D., Koller, S., *et al.* (2005) Confocal examination of untreated fresh specimens from basal cell carcinoma. *Arch. Dermatol.* 141, 1269–1274.

Horn, M., Gerger, A., Koller, S., *et al.* (2007) The use of confocal laser-scanning microscopy in microsurgery for invasive squamous cell carcinoma. *Br. J. Dermatol.* 156, 81–84.

Lieber, C.A., Majumder, S.K., Billheimer, D., Ellis, D.L. & Mahadevan-Jansen, A. (2008) Raman microscopy for skin cancer detection. *J. Biomed. Opt.* 13(024013), 1–9.

Lin, S.J., Jee, S.H., Kuo, C.J., *et al.* (2006) Discrimination of basal cell carcinoma from normal dermal stroma by quantitative multiphoton imaging. *Opt. Lett.* 31, 2756–2758.

Nijssen, A., Maquelin, K., Santos, L.F., *et al.* (2007) Discriminating basal cell carcinoma from preilisional skin using high wave-number Raman spectroscopy. *J. Biomed. Opt.* 12, 034004.

Olmedo, J.M., Warschaw, K.E., Schmitt, J.M. & Swanson, D.L. (2006) Optical coherence tomography for the characterization of basal cell carcinoma in vivo: a pilot study. *J. Am. Acad. Dermatol.* 55, 408–412.

Paoli, J., Smedh, M., Wennberg, A.M. & Ericson, M.B. (2007) Multiphoton laser scanning microscopy on non-melanoma skin cancer: morphologic features for future non-invasive diagnostics. *J. Invest. Dermatol.* 128, 1248–1255.

Patel, Y.G., Nehal, K.S., Aranda, I., Li, Y., Halpern, A.C. & Rajadhyaksha, M. (2007) Confocal reflectance mosaicing of basal cell carcinomas in Mohs surgical skin excisions. *J. Biomed. Opt.* 12, 034027.

Rajadhyaksha, M., González, S., Zavislan, J.M., Anderson, R.R. & Webb, R.H. (1999) In vivo confocal scanning laser microscopy of human skin II: advances in instrumentation and comparison to histology. *J. Invest. Dermatol.* 113, 293–303.

Rajadhyaksha, M., Menaker, G., Flotte, T.J., Dwyer, P.J. & Gonzalez, S. (2001) Rapid confocal examination of non-melanoma cancers in skin excisions to potentially guide Mohs micrographic surgery. *J. Invest. Dermatol.* 117, 1137–1143.

Rajadhyaksha, M., Gonzalez, S. & Zavislan, J.M. (2004) Detectability of contrast agents for confocal reflectance imaging of skin and microcirculation. *J. Biomed. Opt.* 9, 323–331.

Smithpeter, C., Dunn, A., Drezek, R., Collier, T. & Richards-Kortum, R. (1998) Near real-time confocal microscopy of cultured amelanotic cells: sources of signal, contrast agents and limits of contrast. *J. Biomed. Opt.* 3, 429–436.

Stenquist, B., Ericson, M.B., Strandeberg, C., Mölne, L., Rosén, A., Larkö, O. & Wennberg, A.M. (2006) Bispectral fluorescence imaging of aggressive basal cell carcinoma combined with histopathological mapping: a preliminary study indicating a possible adjunct to Mohs micrographic surgery. *Br. J. Dermatol.* 154, 305–309.

Sun, C., Beare, R., Volker, H. & Jackway, P. (2006) Mosaicing of microscope images with global and radiometric corrections. *J. Microsc.* 224, 158–165.

Yaroslavski, A.N., Salomatina, E.V., Neel, V., Anderson, R. & Flotte, T. (2007) Fluorescence polarization of tetracycline derivatives as a technique for mapping nonmelanoma skin cancers. *J. Biomed. Opt.* 12(014005), 1–9.

